Liu *et al.*
Acta Neuropathologica Communications (2025) 13:2
https://doi.org/10.1186/s40478-024-01919-4

Acta Neuropathologica Communications

RESEARCH

Open Access

Gain-of-function *ANXA11* mutation cause late-onset ALS with aberrant protein aggregation, neuroinflammation and autophagy impairment

Qing Liu[1*], Ye Sun[1], Baodong He[1], Haodong Chen[1], Lijing Wang[1], Gaojie Wang[1], Kang Zhang[2,3], Ximeng Zhao[4], Xinzhe Zhang[4], Dongchao Shen[1], Xue Zhang[4,5*] and Liying Cui[1*]

Abstract

Mutations in the *ANXA11* gene, encoding an RNA-binding protein, have been implicated in the pathogenesis of amyotrophic lateral sclerosis (ALS), but the underlying in vivo mechanisms remain unclear. This study examines the clinical features of ALS patients harboring the *ANXA11* hotspot mutation p.P36R, characterized by late-onset motor neuron disease and occasional multi-system involvement. To elucidate the pathogenesis, we developed a knock-in mouse model carrying the p.P36R mutation. In both heterozygous and homozygous mutant mice, ANXA11 protein levels were comparable to those in wild-type. Both groups exhibited late-onset motor dysfunction at approximately 10 months of age, with similar survival rates to wild-type (> 24 months) and no signs of dementia. Pathological analysis revealed early abnormal aggregates in spinal cord motor neurons, cortical neurons, and muscle cells of homozygous mice. From 2 months of age, we observed mislocalized ANXA11 aggregates, SQSTM1/p62-positive inclusions, and cytoplasmic TDP-43 mislocalization, which intensified with disease progression. Importantly, mutant ANXA11 co-aggregated with TDP-43 and SQSTM1/p62-positive inclusions. Electron microscopy of the gastrocnemius muscle uncovered myofibrillar abnormalities, including sarcomeric disorganization, Z-disc dissolution, and subsarcolemmal electron-dense structures within autophagic vacuoles. Autophagic flux, initially intact at 2 months, was impaired by 9 months, as evidenced by decreased Beclin-1 and LC3BII/I levels and increased SQSTM1/p62 expression, coinciding with mTORC1 hyperactivation. Significant motor neuron loss and neuroinflammation were detected by 9 months, with marked muscle dystrophy apparent by 12 months compared to wild-type controls. These findings implicate the gain-of-function *ANXA11* mutation drives late-onset motor neuron disease by early presymptomatic proteinopathy, progressive neuronal degeneration, neuroinflammation, and autophagic dysfunction.

Keywords ANXA11, Amyotrophic lateral sclerosis, Mouse model, TDP-43 proteinopathy, Neuroinflammation, Autophagy

*Correspondence:
Qing Liu
drliuqing@126.com
Xue Zhang
xuezhang@pumc.edu.cn
Liying Cui
pumchcuily@sina.com
Full list of author information is available at the end of the article

Introduction

Amyotrophic lateral sclerosis (ALS) is a fatal neurodegenerative disorder characterized by the progressive degeneration of upper and lower motor neurons. *ANXA11*, recently identified as an ALS causative gene, harbors a low-complexity domain (LCD), akin to other RNA-binding proteins (RBPs) such as *TARDBP* and *FUS* [1]. Mutations in *ANXA11* have been associated with a spectrum of clinical phenotypes, including ALS, ALS with frontotemporal dementia (FTD), ALS with behavioral variant FTD, progressive supranuclear palsy, and inclusion body myopathy [2–6]. These mutations span the amino-terminal (N-terminal) LCD and four Annexin (ANX) domains, observed in both familial and sporadic ALS cases. Variants within the LCD, particularly the p.P36R mutation, a hotspot in ANXA11, are linked to distinct clinical features, including late-onset ALS with or without FTD, with disease onset typically occurring between 64 and 71 years and demonstrating high penetrance [3, 5, 7].

The physiological and pathophysiological roles of ANXA11 remain elusive. ANXA11 has been implicated in intracellular Ca^{2+} homeostasis and stress granule dynamics. It is reported to mediate neuronal RNA transport by tethering RNA granules to actively-transported lysosomes, performing a critical cellular function that is disrupted in ALS [1]. Notably, the age of onset in patients with *ANXA11* mutations parallels that of sporadic ALS, suggesting that ANXA11 mutations may alter the mechanisms leading to ALS. This model offers a unique perspective for investigating the underlying pathways of ALS.

In this study, we generated an *ANXA11*-P36R knock-in mouse model, offering a distinct alternative to existing ALS models. These mutant mice exhibited late-onset motor decline and anxiety-like behavior, partially mirroring the clinical phenotypes of ALS patients with the p.P36R mutation. Additionally, we identified multisystem disease pathology, marked by presymptomatic abnormal proteinopathy in both the central nervous system (CNS) and muscles. The observed motor decline, coupled with progressive neuroinflammation and eventual autophagy failure, delineates the pathological progression in this model. Unlike the commonly used *SOD1*-G93A mice, which display early onset and reduced lifespan, the *ANXA11*-mutant mice present a prolonged survival, making them a valuable tool for extended observation of ALS progression, mechanistic studies, and exploration of potential therapeutic interventions.

Materials and methods

Generation of knock-in mice

To generate the *ANXA11*-P36R knock-in mouse, we employed a CRISPR-Cas9-based approach [8, 9]. Due to the shorter length of the mouse ANXA11 protein, the corresponding residue for human P36 is P35. The donor DNA fragment contained the P35R mutation along with flanking left and right homology arms (Fig. 1). C57BL/6 J (JAX, Stock No. 000664) mouse genomic DNA was used as a template to amplify the homology arms. The donor DNA, along with gRNA (gctacgttatccagcccgatAGG, PAM site capitalized) and Cas9 mRNA, was injected into wild-type C57BL/6 J zygotes, producing F0 founder heterozygous mice. The introduction of the P35R (c.C104G) variant disrupted the protospacer adjacent motif (PAM) sequence, preventing further cleavage at the mutated site. To prevent further cleavage at the mutated site, a synonymous mutation was introduced by substituting the shadowed base T, thereby disrupting PAM recognition (Fig. 1). Offspring with the desired genotype were backcrossed with wild-type C57BL/6 J mice over several generations to establish stable lines. Homozygous mice were generated by crossing heterozygous individuals, and the presence of heterozygous and homozygous knock-in alleles was confirmed by Sanger sequencing. All animal procedures were conducted in accordance with the Institutional Animal Care and Use Committee (IACUC) guidelines at Peking Union Medical College Hospital, adhering to the Guide for the Care and Use of Laboratory Animals (Eighth Edition, NHR). Mice were housed in individually ventilated cages (up to six per cage) in a barrier facility, maintained under a 12/12-h light/dark cycle at 22–26 °C, with 40–70% humidity, and provided with sterile food and water ad libitum. Daily cage checks ensured animal welfare, and body weight was monitored regularly. The study adhered to the 3Rs principles (replacement, refinement, and reduction) in the use of animals.

mRNA and protein analysis

Mice euthanasia was performed by carbon dioxide inhalation followed by decapitation. Forebrain samples (single hemisphere) and gastrocnemius muscle were collected in and flash frozen in liquid nitrogen and kept at − 80 ℃ until use. Total RNA was extracted using TRIzol (Invitrogen). RNA was used for reverse transcriptase PCR according to the Reverse Transcription System (Promega, Madison, WI) instructions. RT-quantitative PCR was performed using qPCR SYBR Green Master Mix (Yeasen Biotechnology) with the primer pair *Anxa11* -F (5'- CCT ATCGGGCTGGATAACGTAG-3') and *Anxa11*- R (5'-CAGACATGTTGGCTGCCATGC-3'). Each reaction was performed in triplicate and the mean Cq value was used for calculation.

For western blot, lysates were mixed with SDS-PAGE sample loading buffer, separated by SDS-PAGE on a 4%-20% polyacrylamide gradient gel, and blotted onto

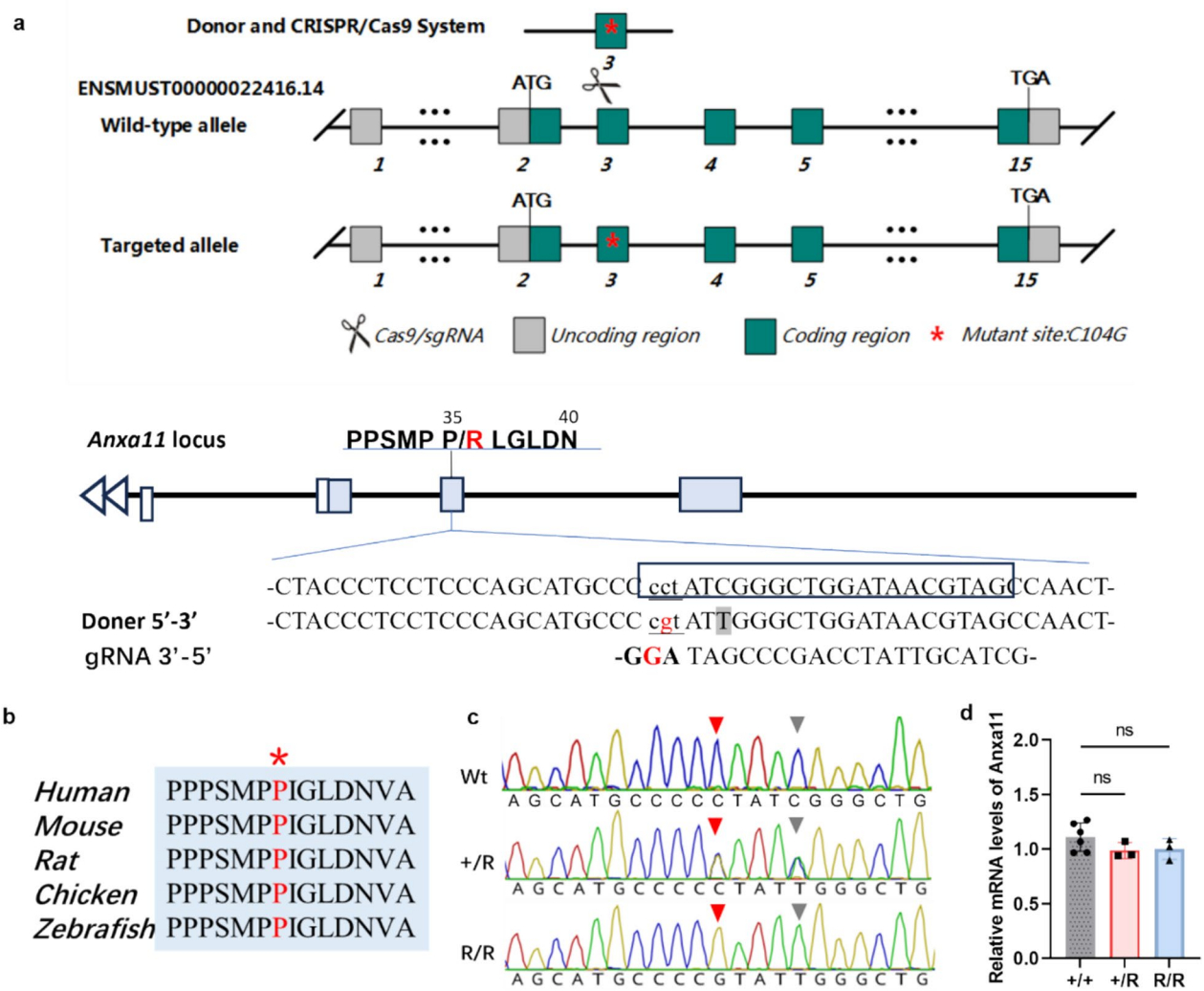

Fig. 1 Generation of the *ANXA11*-P36R knock-in mouse. **a** The genome structure of mouse *Anxa11*. The mouse *Anxa11* P35 corresponds to human P36. The mutant nucleotide was labelled in red. The boxed sequences corresponded to guide RNA (gRNA) sequences. The underlined sequence is the PAM site (bold upper case). A synonymous mutation was introduced by replacing C with T (the shadowed case) to prevent secondary editing. **b** Alignment of amino acid in *ANXA11* around mutant position is highly conserved in different species from human to zebrafish. Human *ANXA11* sequences were used as a reference and the P36 residue is labelled with asterisk. **c** Sanger sequencing of wildtype and knock-in mice. Red triangle arrow showed the mutated residue 104 in wild-type (Wt), heterozygous (+/R) and homozygous (R/R) *ANXA11* mutant mice. Grey triangle arrow showed the created synonymous mutation preventing secondary splice by Cas 9. **d** Expression of *Anxa11* mRNA level in mouse brain. The mRNA expression in both heterozygous and homozygous *ANXA11*-P36R knock-in mice was comparable with that in the wild-type

polyvinylidene fluoride membranes. The membranes were blocked with 5% dry skim milk or 5% bovine serum albumin in tris-buffered saline Tween 20. Antibodies were diluted in a blocking buffer and incubated overnight at 4 °C. Primary antibody details were listed in Supplemented Table 1. Membranes were probed with anti-rabbit or anti-mouse HRP-conjugated IgG. Immunoreactivity was detected using an enhanced chemiluminescence substrate and a Western blot imaging system (Biorad, Germany). Analysis of Western blot signals was performed using Biorad imaging software. Relative expression level of each protein was normalized to GAPDH.

For nuclear and cytoplasmic protein separation, prepare 30 mM Tris–HCl by diluting 1 M Tris–HCl with PBS. Dissolve urea (CAS 57-13-6) in this buffer to prepare a 7 M urea solution, adding 1 × protease and phosphatase inhibitors. Lyse samples with RIPA buffer and centrifuge at 14,000 g for 15 min to collect cytoplasmic proteins. Resuspend the pellet in the urea solution, incubate on ice with intermittent vortexing (5 times, 1 min each), then centrifuge at 14,000 g for 15 min. The

supernatant contains nuclear proteins. GAPDH (Proteintech, #60004-1-Ig, 1:1000) and PCNA (CST, #13110S, 1:1000) were used as cytoplasmic and nuclear controls, respectively.

Co-immunoprecipitation (Co-IP) was performed to examine the interaction between TDP-43 and ANXA11 in mouse brain. Briefly, 1 mg of mouse brain lysate was incubated overnight at 4 °C with anti-TDP-43 antibody-conjugated resin to immunoprecipitate TDP-43 and associated proteins. Immunoprecipitates were analyzed by Western blot using anti-ANXA11 antibody (Proteintech, #10,479–2-AP, 1:3000). The Co-IP Kit (Epizyme, YJ-201) was used following the manufacturer's protocol.

For TDP-43 aggregation analysis, homogenize tissue in TBS buffer (50 mM Tris, 150 mM NaCl, 1 mM EDTA, 1 mM EGTA, protease, and phosphatase inhibitors). Centrifuge at 23,000 rpm (32,000 g) for 15 min to collect the TBS-soluble fraction. Resuspend the pellet in sucrose buffer (0.32 M sucrose, 10 mM Tris–HCl pH 7.4, 0.8 M NaCl, 1 mM EGTA, protease, and phosphatase inhibitors) and repeat centrifugation. Incubate the resulting supernatant with 1% sarkosyl at 37 °C for 1 h, then centrifuge at 60,000 rpm (195,000 g) for 30 min. Collect the supernatant as the sarkosyl-soluble fraction and the pellet as the sarkosyl-insoluble fraction.

Behavioral assessments

All behavioral assessments were performed by a blinded investigator. For heterozygous mice, 7 mutants (male: female = 3:4) and 7 wildtypes (male: female = 3:4) were analyzed. For homozygous knock-in mice, 13 mutants (male:female = 6:7) and 10 wildtypes (male: female = 5:5) at 6-month old, and 8 mutants (male:female = 4:4) and 8 wildtypes (male: female = 4:4) at 10-month old, were analyzed. Data from the behavioral experiment were automatically recorded by a computer system Noldus EthoVision XT9 and completed by two researchers. For evaluation of motor ability, grip strength (DEFII-002, Chatillon, Largo, FL, USA), rotarod (LE8205; Panlab Harvard Apparatus), and wire hang tests were performed monthly from 3 months (mo) of age. For cognitive and mood evaluation, novel object recognition (NOR), Y-maze, open field tests (OFT), and elevated plus maze (EPM) were performed. Body weight was recorded at all time points.

Detailed protocols of behavior tests were described in Supplemented methods and materials. In short, for grip strength, the averages of five trials for bilateral forelimb and hindlimb grip strength were calculated. Wire hang performance was reported as the longest latency to fall time out of three individual trials (maximum time of 2 min). For rotarod performance, the stay time was calculated and the mean value of the stay time from three consecutive trials per day was used for statistical analysis. For OFT, multiple parameters, including total distance, average speed, and distance travelled in the center region were tracked using the TopScan behavioral analysis system (CleverSys) [10]. NOR test assessed short-term recognition memory by comparing the exploration time of new object and familiar object [11]. EPM test was used to measure anxiety-like behavior by calculating the time spent in the open arms [12]. In the Y-maze test, higher spontaneous alternations and more entries into the novel zone indicated better learning and memory ability [13].

Immunostaining and density quantification

For tissue immunostaining, anaesthetized mice were perfused with PBS and then 4% PFA, and brains were post-fixed in the same fixative before paraffin embedding. Antigen retrieval was performed in 0.01 M citrate buffer, pH 6.0. The sections were incubated at 4 °C overnight with the primary antibodies: rabbit anti-ANXA11 (Proteintech, 10,479–2-A,1:400), rabbit anti-ChAT (Proteintech, 20,747–1-AP, 1:200), mouse anti-GFAP (Cell Signaling, #3670, 1:500), rat anti-IBA1(Abcam, EPR16589, 1:200), rabbit anti-TDP-43 (Proteintech, 10,782–2-AP, 1:5000) and rabbit anti-SQSTM1/p62(Novus Biologicals, NBP1-48,320, 1:100).

For immunohistochemistry, sections were washed and incubated with the appropriate biotinylated secondary antibody (Vector, 1:1000), and then with an ABC kit (Vector). Sections were imaged using a Zeiss light microscope. Fluorescent detection was performed with Alexa Fluor-conjugated secondary antibodies (Invitrogen). Images were acquired with a Leica TCS SP8 laser-scanning confocal microscope (Leica). Images were maximum-intensity projected across the z-stack to yield one image representing the entire thickness. For each image, a region of interest (ROI) was created containing ventral horns in each hemisphere of the spinal cord. Example ROIs are provided in each figure. After ROI creation, contrast adjustments were applied to remove the background signal while keeping the punctate intensity at a consistent level across all images. *ANXA11*-mutant animals were individually compared with the average of all wild-type (wt) measurements. For GFAP-positive and IBA1-positive cell count, the number and intensity of positive cells were counted using Imaris. Data were obtained from > 3 images for each animal and each experiment.

Electromyogram acquisition, muscle biopsy, immunohistochemical studies, and imaging

Mice were anesthetized and maintained at 37 °C on a heating pad. Electromyographic (EMG) activity was assessed using concentric needle electrodes

(30 g × 25 mm, Natus, USA) inserted sequentially into the four quadrants of the examined muscle. Compound muscle action potentials (CMAPs) were recorded by placing the stimulation electrode distally to the recording electrode.

For histopathological analysis, snap-frozen gastrocnemius muscle samples from wt and mutant mice were processed using standard techniques, including hematoxylin and eosin (HE) and NADH tetrazolium reductase (NADH-TR) staining [14]. Ultrathin resin Sects. (70–80 nm) were prepared for electron microscopy and examined using a TEM-1400plus transmission electron microscope (40–120 kV). Electron micrographs were acquired with an Olympus-SIS Morada digital camera (Olympus Soft Imaging Solutions, Münster, Germany).

Statistical analysis

Data are presented as mean ± standard error of the mean (SEM). Statistical comparisons were made using GraphPad Prism 7. Independent data with normal distribution and homogeneity of variance were analyzed using Student's *t*-test; non-parametric data were analyzed using the Mann–Whitney test. Group means were compared using one-way ANOVA followed by Tukey's post hoc test. Statistical significance was defined as $p < 0.05$, with significance levels indicated as $^{*}p < 0.05$, $^{**}p < 0.01$ and $^{***}p < 0.001$.

Results

Clinical features of patients with the gain-of-function P36R mutation in *ANXA11*

The p.P36R mutation in *ANXA11* is recognized as a hotspot mutation, first reported by Zhang et al. [5] in three patients with ALS or ALS-frontotemporal dementia (ALS-FTD). To date, ten cases of this mutation have been documented [1, 3, 5]. We summarized the demographic characteristics of these cases (Table 1). The mean age of onset for ALS patients carrying this mutation was 72.3 ± 5.5 years, with an average survival time of 29.6 ± 7.9 months. ALS-FTD was observed in six patients (60%), while three patients (30%) presented with cognitive impairment. The site of disease onset was bulbar in seven patients (70%) and limb in three patients (30%). Additional manifestations, such as bradykinesia and hypophonia, have also been reported in a single FTD patient harboring the p.P36R mutation [15]. Patients with mutations in the low-complexity domain (LCD) of ANXA11 adjacent to P36R also present with inclusion body myopathy [2, 16, 17]. A gain-of-function mechanism has been proposed for *ANXA11* mutations, as ANXA11 expression remains unaltered alongside the observed pathological findings in patients [1]. Overall, *ANXA11*-associated ALS is characterized by a late age of onset and extended survival, with multisystem involvement.

Table 1 Demographic and clinical characteristics of ALS patients with P36R mutation in *ANXA11*

Clinical features	ALS patients with P36R mutation (n = 10)
Male: Female	1:1
Age at onset (years), average ± SD	72.30 ± 5.53
Survival time (months), average ± SD	29.60 ± 7.86
Phenotype	
ALS	1
ALSci	3
ALS-FTD	6
Site of onset, bulbar% (bulbar: limb)	70% (7:3)
Family history, Yes% (Yes: No)	90% (9:1)

ALS amyotrophic lateral sclerosis; *ALSci* amyotrophic lateral sclerosis with cognitive impairment; *FTD* frontal–temporal dementia

Generation of a knock-in mouse line carrying the *ANXA11*-P36R mutation

The P36R mutation in *ANXA11* is located in the LCD and the amino acid is conserved across species (Fig. 1A, 1B). The mouse position corresponding to human P36 is P35. The position is a PAM site for Cas9 recognition. The correct sequence (P35 to R) was introduced and germ line transmission was confirmed after genome editing (Fig. 1C). The *Anxa11* mRNA expression level was comparable with that of wt either in heterozygous (het, + /R) or homozygous (hom, R/R) mutant mice in cortex (Fig. 1D). The protein level of mouse ANXA11 was not affected compared with that of the wt in cortex and muscle of mutant mice in both het and hom mice (Supplemented Fig. 1). Also, homologous PCR products with primers located in exon 1 and exon 4 of *Anxa11* showed that no splicing mutation was introduced. We therefore conclude that a knock-in mouse line carrying the ALS *ANXA11*-P36R mutation is established.

ANXA11-P36R knock-in mice exhibit late-onset motor neuron disease

Similar to the late-onset motor disability and extended life expectancy observed in ALS patients carrying *ANXA11* mutations [14] (Table 1), *ANXA11*-P36R knock-in mice demonstrated significant motor decline at 10 months (mo) of age in both het and hom animals (Fig. 2; Supplementary Fig. 2) compared to wt mice, with no evident impairment in younger mice (6 mo; Supplementary Fig. 3). Paralysis was not observed up to 12 mo of age, although occasional hindlimb spasms were noted. Mutant mice displayed reduced limb stretching when

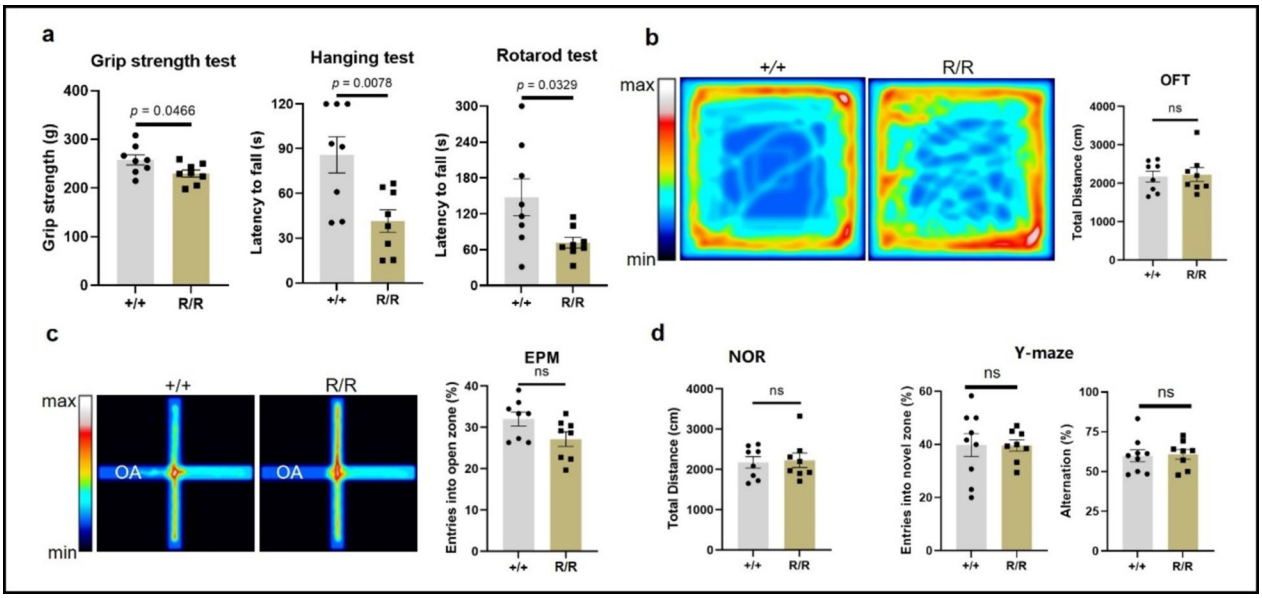

Fig. 2 Motor and cognitive performance of 10-month-old homozygous *ANXA11*-P36R knock-in mice. **a** Motor decline in homozygous (R/R) mutant mice compared with wild-type (+/+). Mutant mice showed reduced grip strength ($p = 0.0466$), shorter hanging endurance time ($p = 0.0078$), and decreased retention time on the rotarod test ($p = 0.0329$) compared with wild-type. **b** Representative heatmap and results from the open field test with no significant difference between the two groups. **c** The results from the elevated plus maze. Homozygous *ANXA11*-P36R knock-in mice displayed tendency of anxiety-like behavior with no significance compared with wild-type ($p = 0.052$). **d** Dementia was not evident in homozygous 10-month-old mutant mice. The percentage of time spent investigating a novel object (left, NOR), and the number of entries into the novel arm and spontaneous alternation (right, Y maze) showed no significant differences between wild-type and mutant mice. Data are presented as mean ± SEM (n = 8 mice per group), with statistical analysis performed using Student's unpaired *t*-test

suspended by the tail compared with wt mice. Behavioral tests revealed reductions in grip strength and spontaneous locomotor activity in het mice compared with wt (Fig. 2a, b). Hanging endurance time and rotarod performance further indicated diminished motor ability (Fig. 2a). No differences were observed in disease onset or progression speed between het and hom mice, although spasms were more frequent in hom mice from 8–9 mo onward (Supplementary Fig. 4). The knock-in mice also exhibited prolonged survival, with no disease-related mortality observed during a 24-mo observation period; one mouse died due to injury, and one from unknown causes shortly after birth. Overall, *ANXA11*-P36R mutant mice exhibited relatively mild disease progression without severe paralysis.

Electromyography reveals early neurogenic impairment in *ANXA11*-P36R knock-in mice. Electromyographic assessments were performed on hom ANXA11-P36R knock-in mice and their wt littermates at 2, 4, 10, and 12 months of age. Denervative potentials were first detected in multiple skeletal muscles at 2 months, although CMAP amplitudes remained normal at this stage. By 4 months, mutant mice exhibited abundant fibrillations, positive sharp waves, and spontaneous and giant motor unit potentials across muscles in multiple spinal cord segments, which were scarcely observed in wt littermates (Fig. 3a). Both mutant and wt mice showed motor development from 4 to 10 months, as indicated by increased CMAP. However, mutant mice exhibited a significant decline in baseline-to-peak (B-P) and peak-to-peak (P-P) CMAP amplitudes, with a more pronounced decrease in hindlimbs compared with forelimbs. Notably, a significant reduction in CMAP was first observed in hindlimbs at around 4 months, and in forelimbs at around 10 months (Fig. 3b). These findings suggest early and extensive neurogenic impairment, characteristic of ALS in patients.

Intact working memory was observed in het and hom *ANXA11*-P36R knock-in mice. To assess FTD-like symptoms, we conducted NOR, Y-maze, and EPM tests. During NOR tasks, both het and hom mice explored objects equally with wt, indicating no difference in novelty discrimination (Fig. 2d, Supplemented Fig. 2d). In the Y-maze test, there was no significant difference in the number of entries into the novel arm or in spontaneous alternations between het and wt, as well as between hom and wt mice (Fig. 2d, Supplemented Fig. 2d). However, at 10 months, het knock-in mice displayed anxiety-like behavior, with significantly fewer entries into the open arms during the EPM test compared with wildtype mice

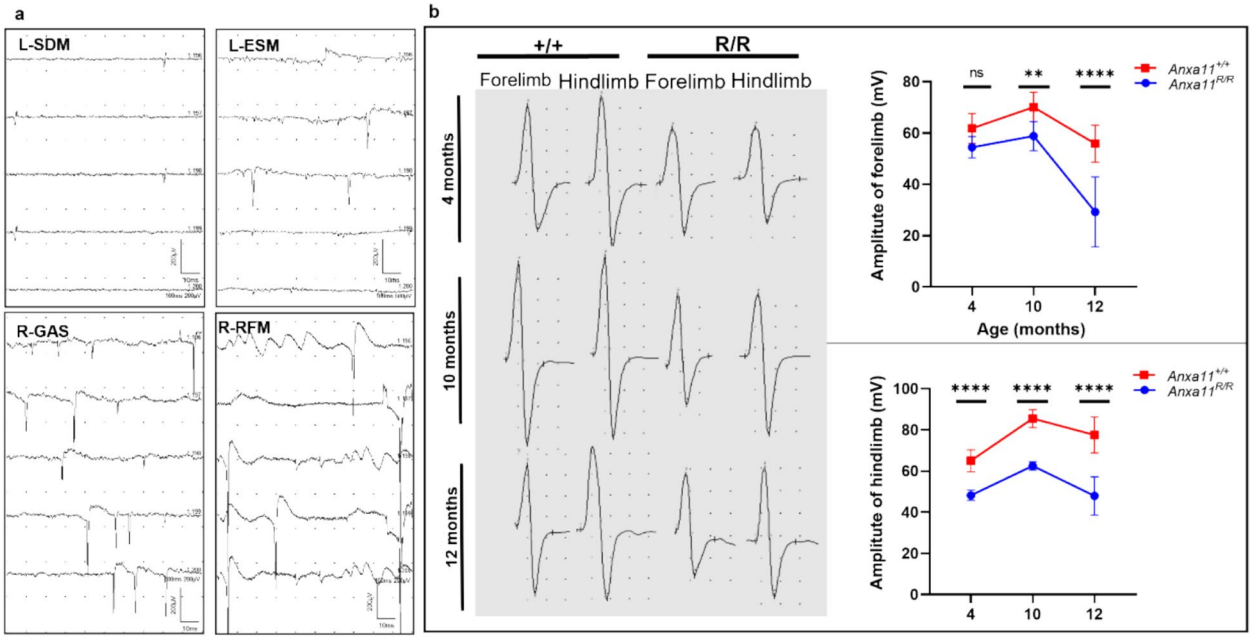

Fig. 3 Electromyography of homozygous *ANXA11*-P36R knock-in mice. **A** Representative images of denervative potentials detected in mutant mice, including fibrillation potentials in the left shoulder-deltoid muscle (SDM), positive sharp waves (PSWs) in the left erector spinae muscle (ESM) and right gastrocnemius muscle (GAS), and spontaneous and giant motor unit potentials in the right GAS and right rectus femoris muscle (RFM). **B** Representative CMAP responses in the forelimbs and hindlimbs of wild-type (+/+) and mutant (R/R) mice. Left, representative CMAP images in wild-type and mutant mice at different ages. Right, peak-to-peak CMAP amplitudes in wild-type and mutant mice. Both mutant and wild-type mice exhibited motor development from 4 to 10 months. CMAP amplitudes decreased significantly in mutant mice over time, particularly in hindlimbs from 10 to 12 months, whereas amplitudes remained stable in wild-type mice (Two-way ANOVA with Sidak's multiple comparisons test, $*p<0.05$, $**p<0.01$, $***p<0.001$, $****p<0.0001$; $n=3$ mice per group)

($p<0.01$; Fig. 2c). Hom mice showed a decreasing trend with no statistically significant difference ($p=0.052$) compared with the wt in the open arm entry frequency (Supplementary Fig. 2). These findings indicate that *ANXA11*-mutant mice do not exhibit dementia but display a propensity for anxiety-like behavior.

We thus conclude the established *ANXA11*-P36R knock-in mice recapitulates key phenotypes of ALS patients, including late-onset motor decline and preserved lifespan.

Early aberrant protein aggregation in the central nervous system of *ANXA11*-P36R mice

In ALS patients with *ANXA11* mutations, ANXA11 forms diverse and heterogeneous aggregates, which are believed to contribute to neurodegeneration [18]. In the *ANXA11*-P36R knock-in mouse model, we observed early aggregates of mutant ANXA11 in the cytoplasm of spinal cord motor neurons (MNs) at 2 months of age (Fig. 4a). These aggregates co-localized with SQSTM1/p62-positive inclusions (Fig. 4a), which are associated with oxidative stress, the ubiquitin–proteasome system, and the autophagy pathway [19, 20]. In wt littermates, ANXA11 was homogeneously dispersed in the nucleus and cytoplasm, and SQSTM1/p62 protein did not form aggregates (Fig. 4a; Supplementary Fig. 5). The co-localization of mutant ANXA11 aggregates with SQSTM1/p62 inclusions became increasingly prominent in spinal cord MNs as the disease progressed (Fig. 4a). Also, in 4-month-old hom mice, mutant ANXA11 aggregates co-localized with SQSTM1/p62 inclusions in the cortical neuron (Supplementary Fig. 5).

TDP-43 proteinopathy and ANXA11-TDP43 interaction in *ANXA11*-P36R knock-in mice

Mislocalization of TDP-43 is a hallmark of ALS pathology, typically remaining nuclear under normal conditions but translocating to the cytoplasm in neurodegenerative diseases [21]. Unlike *SOD1*-related ALS, which does not always exhibit TDP-43 proteinopathy [22], *ANXA11*-P36R knock-in mice displayed TDP-43 mislocalization in the anterior horn of the mouse spinal cord and cortical neurons (Fig. 4b, c, supplemented Fig. 5). We also extracted proteins from the cytoplasm and the nucleus, respectively, for verification. The evaluation of the cellular localization of TDP-43 showed that the level of cytoplasmic TDP-43 in *ANXA11*-mutant mice increased

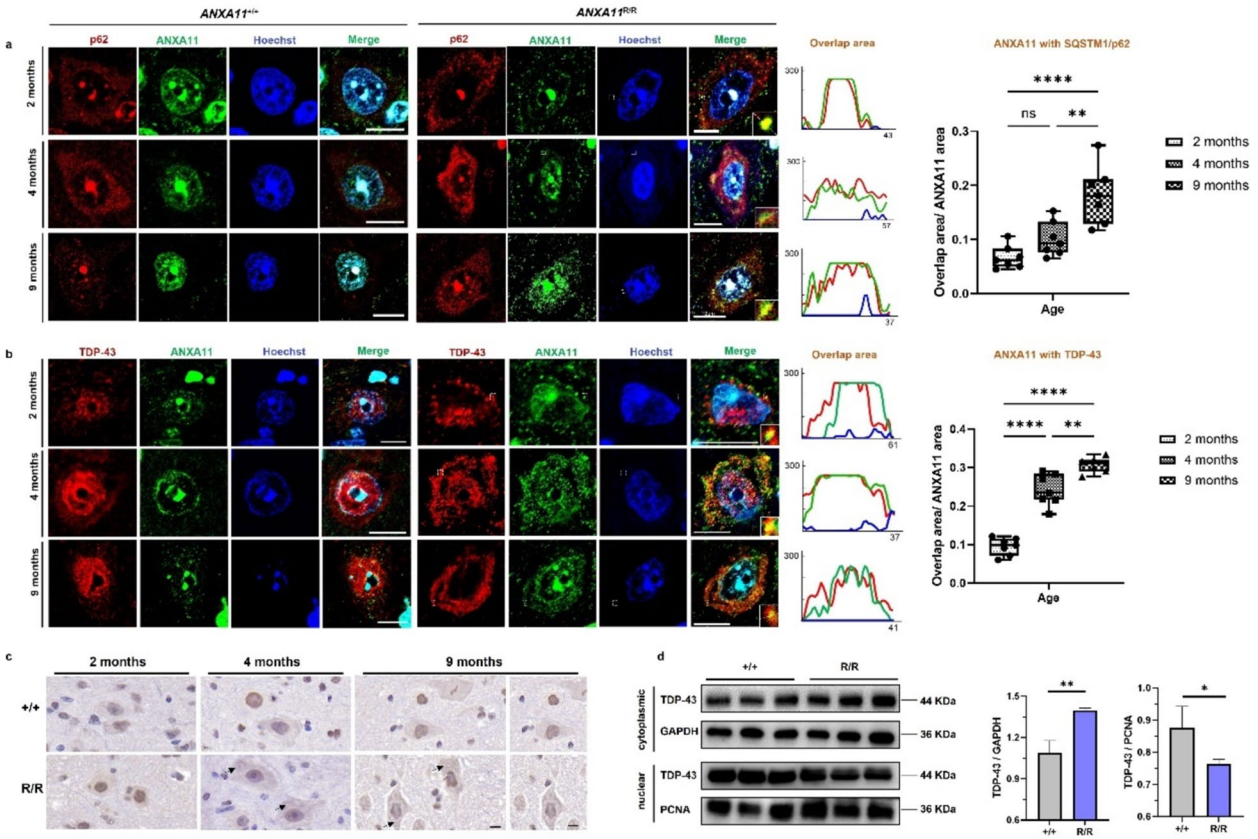

Fig. 4 Early abnormal protein aggregation in central nervous system. **a** Representative fluorescence images show ANXA11 (green) and p62 (red) aggregates in wild-type (+/+) and mutant (R/R) mice at various ages in spinal cord motor neurons. In mutant mice, ANXA11 aggregates are evident in the cytoplasm, co-localizing with SQSTM1/p62-positive clumps from 2 months of age, with increased prominence as the disease progresses (right). Line-scan plots depict the extent of ANXA11 and p62 co-localization. **b** Representative fluorescence images of ANXA11 (green) and TDP-43 (red) aggregates in wild-type (+/+) and mutant (R/R) mice at different ages. TDP-43 mislocalization from the nucleus to the cytoplasm, partially co-localizing with ANXA11 aggregates, is observed in an age-dependent manner in mutant mice. Line-scan plots (right) illustrate a significant increase in ANXA11 and TDP-43 co-localization in mutant mice from 4 months onwards. **c** DAB (3,3′-diaminobenzidine) staining showed translocation of TDP-43 from nucleus to cytoplasm from 4 months on in the brain of homozygous (R/R) mutant mice. **d** Western blotting of nuclear and cytosolic fractions from brains demonstrated an increase in cytosolic TDP-43 levels in homozygous (R/R) mutant mice compared to wild-type (+/+). GAPDH was used as the marker for the cytosolic fraction, and PCNA for the nuclear. Hoechst was used to label nuclei. Scale bars, 10 µm. $N = 3$ mice, $n = 7$ sections *per* group. $^{*}p < 0.05$, $^{**}p < 0.01$, $^{***}p < 0.001$, $^{****}p < 0.0001$

significantly, and the level within the nucleus decreased remarkably (Fig. 4d).

TDP-43 can be found within axonal transporting granules where annexin A11 tethers these ribonucleoprotein granules to lysosomes [23, 24] and ANXA11 aggregates were shown to comingle with TDP-43 in CNS neurons [25, 26]. In our *ANXA11*-mutant mice, from 2 months of age, spinal motor neurons exhibited cytoplasmic TDP-43 inclusions around the nucleus, co-aggregating with mutant ANXA11 (Fig. 4b). By 9 months, nearly all TDP-43 had translocated to the cytoplasm, forming co-aggregates with ANXA11, indicating that pathogenic *ANXA11* mutations induce TDP-43 proteinopathy, which worsens as the disease progresses (Fig. 4b). To further verify whether TDP-43 and ANXA11 interacted with each other, co-immunoprecipitation was conducted. Pulldown of TDP-43 and its interacting proteins showed detection of ANXA11, which indicates direct interaction between TDP-43 and ANXA11 in the pathological state. (Supplementary Fig. 6).

To evaluate the aggregation status of TDP-43 in the brains of *ANXA11*-mutant mice, Western blotting was employed to examine protein samples in the TBS-soluble, sarkosyl-soluble, and sarkosyl-insoluble fractions. Monomeric TDP-43 levels were comparable between wild-type and mutant mice in TBS- and sarkosyl-soluble fractions (n = 3 per group). Sarkosyl-insoluble fractions showed significantly elevated monomeric TDP-43 in

mutant mice, indicating increased aggregation (Supplementary Fig. 7).

Inclusion body myopathy in *ANXA11*-P36R knock-in mice

Patients with *ANXA11* mutations present with inclusion body myopathy (IBM) [2], which we recapitulated in our mutant mice model. No muscle dystrophy was evident until 9 months of age in mutant mice (Fig. 5a). Moreover, the gastrocnemius muscle of the *ANXA11*-mutant mice exhibited grouped muscle atrophy (Supplementary Fig. 8). Nuclear centralization, moth-eaten intermyofibrillar structures, and rimmed vacuoles with eosinophilic inclusions were observed, exhibiting features similar to those in *ANXA11*-mutant patients [16, 26]. Notably, at 2 months, while muscle cells appeared intact under HE staining, immunofluorescence detected fine particles of mutant ANXA11 in the sarcoplasm and sarcolemma. By 4 months, these particles had progressed to small aggregates co-localizing with TDP-43 inclusions (Fig. 5b). This novel finding suggests that cerebral cortex, spinal cord, and muscles are all affected early in *ANXA11*-mutant ALS, underscoring the potential diagnostic value of early muscle biopsy.

Electron microscopy revealed myofibrillar disorganization, Z-disc dissolution, and subsarcolemmal autophagic material in mutant mice (Fig. 5c), consistent with patient biopsies [16, 17, 26]. Subsarcolemmal osmophilic structures and vacuoles, resembling myelin-like debris or remnant organelles, were also observed. Lipid and mitochondrial droplets were noted at the vacuole periphery (Fig. 5c). These findings indicate that *ANXA11*-P36R ALS is a multisystem disorder characterized by TDP-43 proteinopathy.

Late motor neuron degeneration and neuroinflammation in *ANXA11*-P36R knock-in mice

In addition to impaired motor abilities, *ANXA11*-P36R knock-in mice exhibit progressive MN degeneration, detectable by 4 months (Fig. 6a). Alongside a reduction in ChAT-positive MNs in the anterior horn of the spinal cord, mutant MNs exhibit larger somas and fewer dendrites (amplified images, Fig. 6a). Significant MN loss was observed by 9 months compared to wild-type siblings (Fig. 6a, ChAT histogram), indicative of neuronal degeneration.

Neuroinflammation, marked by increased GFAP- and IBA1-positive cells, was detected early in mutant mice (Fig. 6b, 6c). GFAP and IBA1 expression was significantly elevated in homozygous mutants from 4 months, becoming pronounced by 9 months (Fig. 6a, GFAP & IBA1 histograms). During reactive astrogliosis, GFAP is upregulated, mirroring an increase in both astrocyte number, size and processes [27]. Reactive astrocytes exhibited nuclear translocation of NF-κB (Supplementary Fig. 9a), indicating an inflammatory state influences disease pathogenesis in the current model of ALS. Similarly, mutant microglia showed elevated IBA1 levels and an amoeboid morphology (Supplementary Fig. 9b), a characteristic of neuroinflammation [28]. The *ANXA11*-P36R knock-in ALS model thus displays late MN degeneration and neuroinflammation associated with disease progression.

Mutant ANXA11 is associated with autophagy impairment and activated mTOR signaling

Given ANXA11's role in RNA granule transport and its interactions with lysosomes, we explored autophagic dysfunction as a potential mechanism underlying the P36R mutation. Autophagy markers were analyzed in the lumbar spinal cord of 2-, 4-, and 9-month-old mice. Autophagy initiation marker Beclin-1(BECN) and autophagosome formation marker LC3 were normal at 2 months but decreased with disease progression (Fig. 7). Conversely, the autophagy degradation marker p62 showed a progressive accumulation. At 9 months, *ANXA11*-P36R knock-in mice exhibited significantly more neurons and muscle cells with cytosolic p62- and ANXA11-positive inclusions than wild-type siblings (Figs. 4 and 5), demonstrating a loss of autophagic compensation as the disease advanced.

(See figure on next page.)

Fig. 5 Muscle pathology findings in homozygous *ANXA11*-mutant mice. **a** Hematoxylin and eosin (HE) staining of gastrocnemius muscle in wild-type and mutant mice. Muscle fibers in 2-month-old wild-type (+/+) and mutant (R/R) mice were intact (left), with inclusion body myopathy becoming evident from 4 months onward (middle), as indicated by occasional dense sarcoplasmic eosinophilic aggregates (black arrow). By 9 months, mutant mice showed marked muscular dystrophy, nuclear centralization, rimmed vacuoles, and eosinophilic inclusions. *N* = 3 mice. Scale bar, 20 μm. **b** Immunofluorescence of muscle fibers stained for ANXA11 and TDP-43. In 4-month-old mutant muscle cells, ANXA11 aggregates dispersed in the sarcoplasm and sarcolemma, co-localized with TDP-43 inclusions. Scale bar, 20 μm. **c** Ultrastructural findings in *ANXA11*-P36R-associated myopathy. Longitudinal sections of muscle fibers show normal structures in wild-type mice, subsarcolemmal autophagic material in 4-month-old mutants, and Z-disc dissolution with vacuole formation in 9-month-old mutants. Middle panels show subsarcolemmal electrodense structures in small vacuoles (arrow) in 4-month-old homozygous mutants. Bottom panels show autophagic vacuoles with myelin-like debris or remnant organelles in 4- and 9-month-old muscle cells. Scale bars, 1 μm–500 nm (as indicated). Black frames in (a) and white frames in (b) & (c) denote enlarged areas

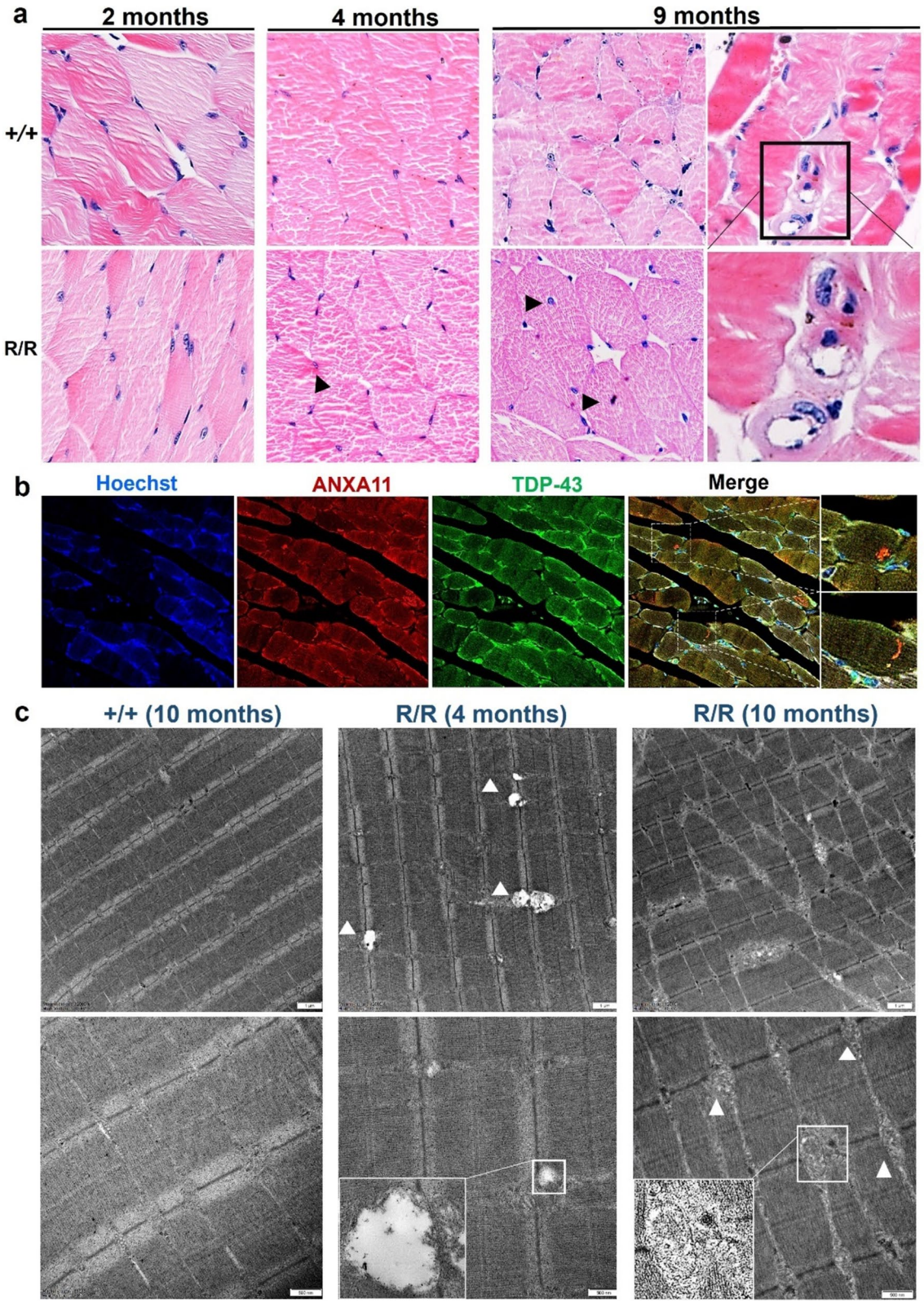

Fig. 5 (See legend on previous page.)

MTOR pathway activation in *ANXA11*-P36R knock-in homozygous mice.

Concurrent with autophagy impairment, the Akt/mammalian target of rapamycin (mTOR) signaling pathway, a key modulator of autophagy [29], was increasingly activated in 9-month-old mutant mice. Elevated ratios of phosphorylated mTOR (S2448) to total mTOR were observed, alongside significant increases in mTORC1-dependent phosphorylation of RPS6KB1/S6K (p70 S6K) (Fig. 8), indicative of mTORC1 activation. Additionally, as mTORC1 activation requires recruitment to lysosomal membrane as well as phosphorylation by the upstream kinase AKT [30], we examined the phosphorylation of AKT (p-AKT) at Ser473. The level of p-AKT was significantly elevated (Fig. 8), further supporting Akt/mTORC1 pathway activation. These data suggest that as the disease progresses, the Akt/mTORC1 pathway becomes increasingly activated, paralleling autophagy impairment and motor decline.

In summary, we generated the first *ANXA11*-P36R knock-in mouse model, providing detailed insights into the phenotypic progression and pathological evolution of *ANXA11*-associated ALS. Our findings demonstrate that the *ANXA11*-P36R variant is sufficient to induce a progressive, age-dependent motor neuron disease with inclusion body myopathy in mice. This model recapitulates key features of ALS, including early abnormal protein accumulation, progressive motor neuron loss with neuroinflammation, and late-stage autophagy impairment and mTOR pathway activation (Fig. 9). The extended presymptomatic interval and prolonged survival of this model make it a valuable tool for mechanistic studies and therapeutic interventions in ALS.

Discussion

We here provide both clinical and in vivo data based on an ALS/FTD-associated *ANXA11* missense mutation. Developing animal models that accurately represent human disease has been a longstanding priority within the ALS research community. The *ANXA11*-P36R knock-in mouse model established here provides a novel in vivo platform for investigating ALS mechanisms. This model recapitulates key behavioral impairments reminiscent of ALS manifestations observed in patients carrying the mutation. Classical ALS mouse models, such as the widely used *SOD1*-G93A model, typically exhibit early disease onset, rapid progression, and short survival time, with disease onset around 2.5 months and rapid decline within 2 months [31]. Notably, *ANXA11* mutations, including the P36R hotspot mutation associated with phenotypes ranging from pure ALS to ALS-FTD, are characterized by a later onset compared to other ALS-associated mutations [3] In our knock-in mice, motor decline manifests after 10 months in both heterozygous and homozygous animals, without evidence of dementia. Pathological changes, however, appear as early as 2.5–3 months, indicating a prolonged presymptomatic phase before motor decline. This model thus represents a slow yet representative paradigm of ALS with steady accumulation of pathology over an extended period, offering a longer window for in vivo drug testing compared to the *SOD1*-G93A model [31]. Furthermore, the survival of *ANXA11*-P36R knock-in mice exceeds 24 months, with no evident paralysis suggesting a mild disease course despite progressive pathology.

Though ALS shares a close clinical and pathological association with FTD [32], in our study, *ANXA11*-mutant mice did not demonstrate significant cognitive decline. While heterozygous mice displayed anxiety-like behaviors, homozygous mutants did not show statistically significant differences compared with wild-type controls. These findings suggest that behavioral variant FTD (bvFTD) is relatively infrequent as reported [32] and may not represent a predominant phenotype in *ANXA11*-mutant mice. Overall, the *ANXA11*-P36R knock-in mice align with the late onset and extended survival observed in patients.

We provide evidence of aberrant protein aggregation at the presymptomatic stage and late autophagy collapse in *ANXA11*-P36R knock-in mice, coinciding with motor decline. In 2-month-old mutant mice, abnormal protein aggregates were detected in both CNS and muscle fibers. In the muscles of patients with ALS, dense filamentous and short linear inclusions as well as group muscle atrophy can be observed [33]. Meanwhile, the muscle pathology exhibited by mouse models is highly similar to that of

(See figure on next page.)

Fig. 6 Neurodegeneration and neuroinflammation in the lumbar spinal cord of homozygous *ANXA11*-P36R knock-in mice. **a** Motor neurons (MNs) in the anterior horn of the spinal cord. MN numbers in homozygous mutant mice (R/R) declined compared with wild-type (+/+) in 4-month and 9-month mice. Mutant MNs exhibited larger somas and fewer dendrites (amplified images, upper right). Histograms show a reduction in ChAT-expressing MNs. Representative images of GFAP-positive astrocytes **b** and IBA1-positive microglia **c** in the ventral spinal cord. Reactive astrocyte and microglial populations increased with disease progression in 2-, 4-, and 9-month-old mutant mice compared with wild-type. The loss of MNs and increase in reactive glial cells became significant in 9-month-old mutants. $N = 3$ mice, $n = 12$ sections *per* group. Scale bar, 200 µm. Data represent mean ± SEM; statistical analysis by *t*-test. $^{*}p < 0.05$

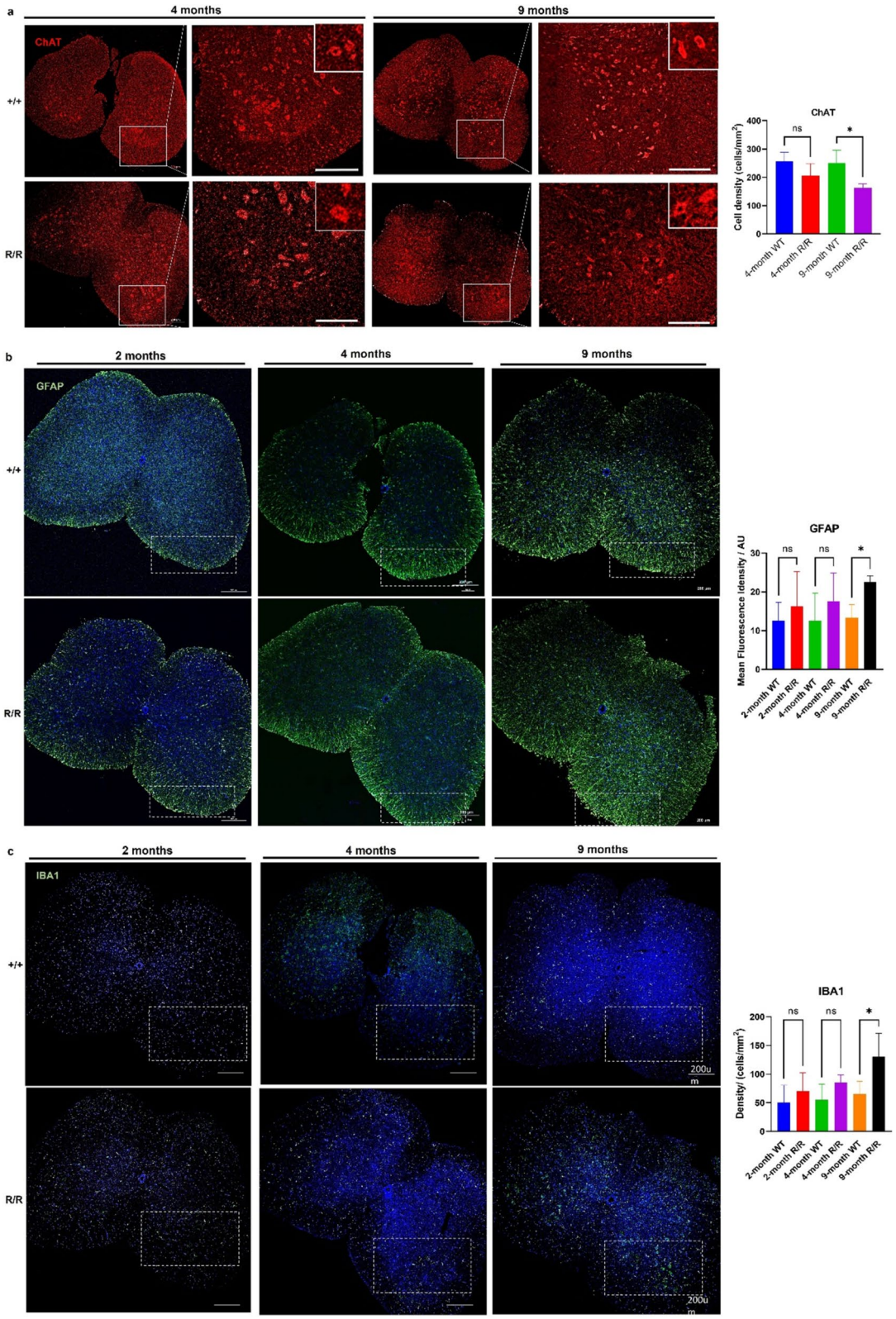

Fig. 6 (See legend on previous page.)

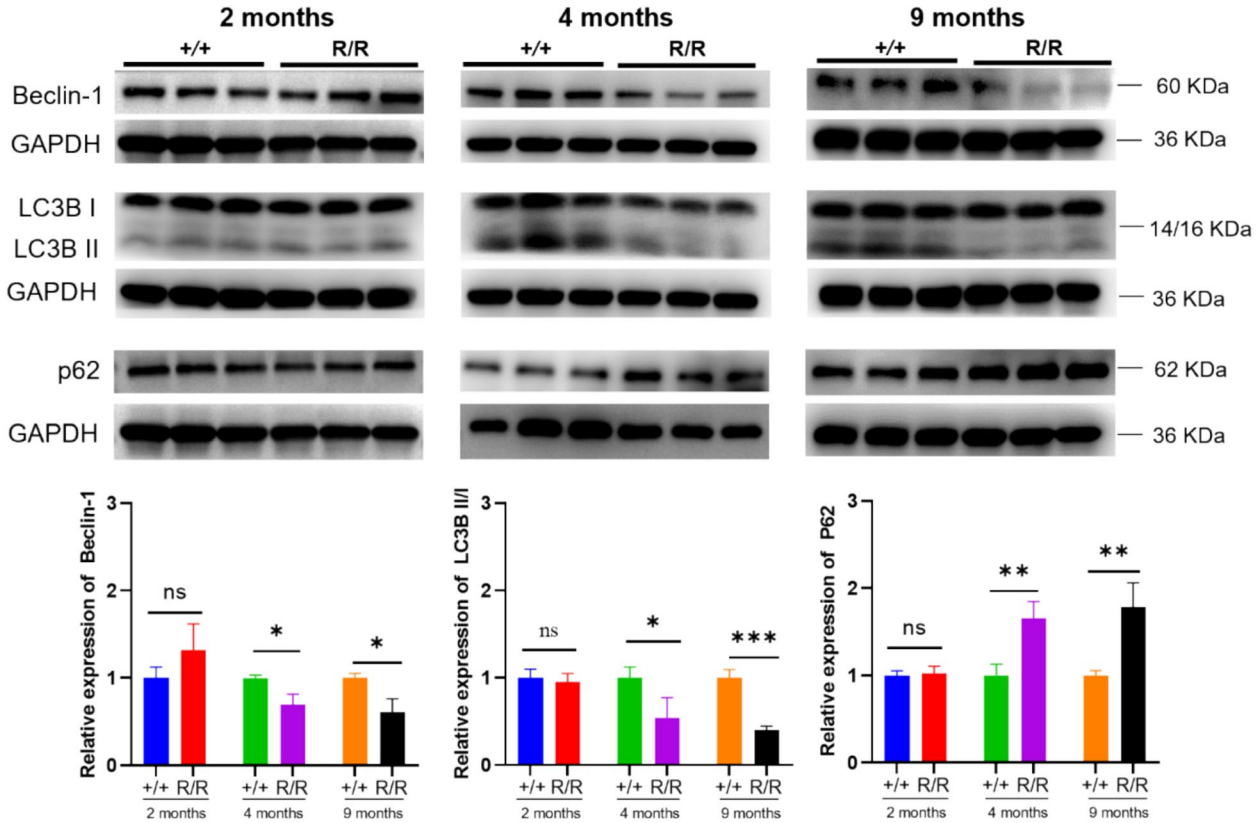

Fig. 7 Progressive autophagy impairment in homozygous *ANXA11*-P36R knock-in mice. Autophagy markers, including Beclin-1, LC3BII/I, and p62, were analyzed in the cortex of 2-, 4-, and 9-month-old mutant mice, revealing a progressive decline in autophagic activity. Representative immunoblots demonstrate the impairment of autophagy in mutant mice, with quantified levels normalized to GAPDH. Statistical analysis was conducted using one-way ANOVA, with data presented as mean ± SEM ($n = 4$ biologically independent replicates *per* group). Significance levels: $^{*}p < 0.05$, $^{**}p < 0.01$, $^{***}p < 0.001$

ALS patients [33, 34], with obvious muscular dystrophy, nuclear centralization, rimmed vacuoles, eosinophilic inclusions and group muscle atrophy. Motor neuron degeneration, and neuroinflammation occurred later, in tandem with motor decline. Several ALS-related genes, such as *OPTN*, *C9orf72*, *SQSTM1*, and *VCP*, are functionally linked to autophagy pathways [35], extending the relevance of findings in *ANXA11*-P36R knock-in mice to a broader context of ALS pathogenesis. Stress granule (SG) formation is a common pathological feature in these ALS models. SGs are membrane-less organelles formed through liquid–liquid phase separation (LLPS) under stress conditions such as oxidative stress and heat shock [36, 37]. While SGs typically undergo dynamic assembly and disassembly, chronic stress can lead to persistent SGs and subsequent aggregation of disease-related proteins. Aggregation of ALS-associated mutant proteins, including SOD1, FUS, and hnRNPA1, has been observed in some patients, with many of these proteins being components of SGs [36, 38–40]. Importantly, prolonged stress can induce aggregation of SG components [41], suggesting that proteins like TDP-43 and FUS may aggregate in ALS via SG assembly. This is also observed in *ANXA11*-P36R knock-in mice, where mutant ANXA11 co-localizes with SGs, and impaired SG clearance indicates associated deficits in protein homeostasis. Unlike typical SGs that form upon stimulus [42], mild SG formation occurred autonomously in *ANXA11* mutant mice. Future studies will involve in vivo stimulation to accelerate disease progression and further elucidate underlying etiologies.

TDP-43 proteinopathies are pathological hallmarks in ALS/FTD [43]. Typical alterations include TDP-43 protein translocation from nucleus to cytoplasm, and increasing motor neuron degeneration accompanied by astrogliosis and microgliosis. It appeared in ~ 98% of ALS and 40% of FTD [44]. Experimental studies using cell culture and animal models have provided supportive evidence that TDP-43 proteinopathies are highly involved in the onset and progression of motor neuron diseases [45]. For example, transgenic mice overexpressing TDP-43 with either familial or sporadic

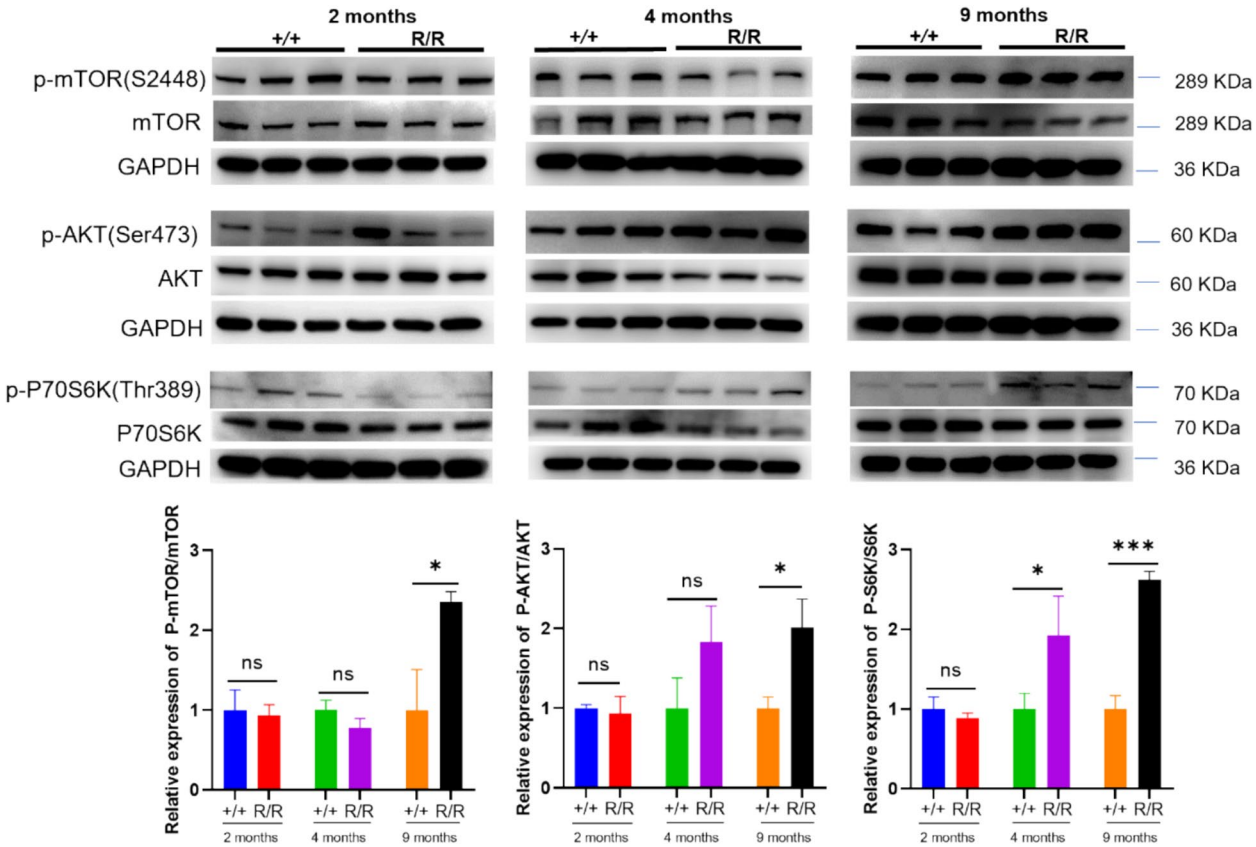

Fig. 8 MTOR activation in homozygous *ANXA11*-P36R knock-in mice. In the cortex of 2-month-, 4 month- and 9-month-old mutant mice, mTOR pathway was activated indicated by elevated p-mTOR/mTOR, p-AKT/AKT, and p-P70S6K/P70S6K levels. Representative immunoblots illustrate these alterations, with data presented as mean ± SEM ($n = 4$ biologically independent replicates *per* group). One-way ANOVA was used to determine statistical significance. *$p < 0.05$, **$p < 0.01$, ***$p < 0.001$

ALS mutations develop a disease-like phenotype [45]. Turning off TDP-43 nuclear localization signal or suppression of mutant TDP-43 expression rescues neurons even after neurodegeneration onset and reversed motor deficits in animal models of the ALS/FTD [46, 47]. But not all ALS have TDP-43 proteinopathies, *SOD1*-mutated patients and mouse model commonly lack of TDP-43 pathology [22]. Furthermore, ANXA11 directly interacts with TDP-43, a conclusion supported by multiple lines of evidence. A recent study by Arseni D et al. revealed the formation of heteromeric amyloid filaments comprising ANXA11 and TDP-43 utilized cryo-electron microscopy in the histopathological analysis of FTLD-TDP Type C [48]. TDP-43 and ANXA11 were co-assembled via their respective LCDs, providing compelling structural insights into their interaction. Our findings also demonstrate this interaction through co-localization studies and Co-IP experiments. Overall, we show that the *ANXA11*-P36R knock-in mouse model has early TDP-43 proteinopathy which may be suitable for small molecule-based or gene-based therapies targeting this common process in future [43].

Disrupted autophagy and proteostasis play a key role in the pathogenesis of ALS. The conserved autophagy pathway is particularly crucial in mitigating pathogenic insults that can precipitate neurodegeneration [48]. Molecular and histopathologic analyses of patient tissues demonstrate mislocalized or accumulated autophagy machinery underlying neurodegenerative diseases. In ALS, pathological inclusions in motor neurons are often surrounded by LC3 and SQSTM1, indicating failed or stalled autophagic clearance [49]. SQSTM1 levels, which inversely correlate with autophagy efficiency, are frequently used to estimate autophagy flux [50]. In our *ANXA11*-mutant mice, SQSTM1 levels increased and SQSTM1 aggregated when autophagy failed. Moreover, the frontotemporal cortex and spinal cord in sporadic ALS patients reveals that ubiquitin-positive inclusions contain TDP-43 [44]. We observed early co-aggregation of mutant ANXA11 with SQSTM1/p62 and TDP-43,

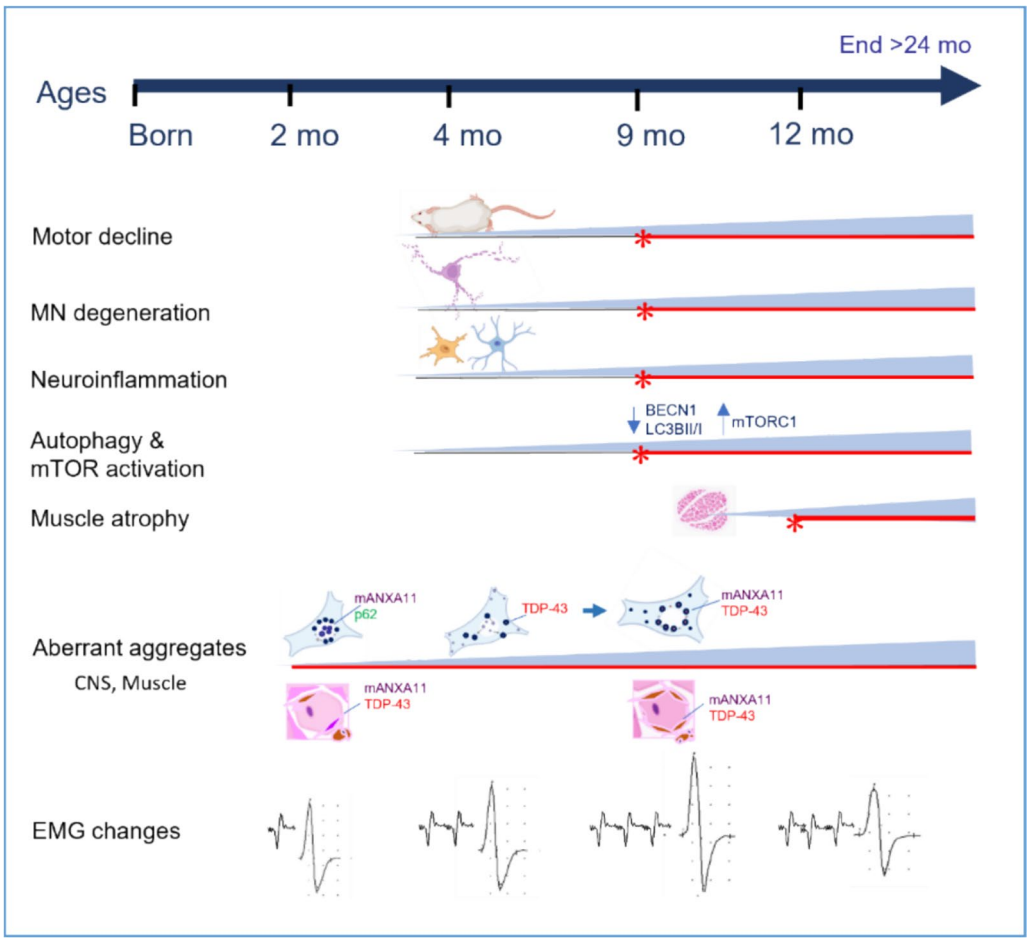

Fig. 9 Summary of pathological and phenotypic progression in *ANXA11*-P36R knock-in ALS mice. The pathological and phenotypic progression in *ANXA11*-P36R knock-in ALS mice is characterized by early abnormal protein aggregation, motor neuron degeneration, neuroinflammation, and autophagy deficits. At 2 months, abnormal protein aggregates were detected in the central nervous system and muscles, accompanied by spontaneous electromyographic activity. Mutant ANXA11 translocated from the nucleus to the perinuclear region, co-aggregating with p62 and TDP-43. Motor neuron degeneration, including neuronal loss and morphological changes, became pronounced by 9 months, alongside neuroinflammation marked by glial activation and NF-κB translocation. Autophagy deficits, indicated by decreased levels of BECN1 and LC3BII/I, were synchronous with motor decline. Muscle atrophy began to appear from 9-months on and was evident by 12 months, though *ANXA11*-mutant mice survived beyond 24 months

with autophagy collapse becoming evident as motor deficits became significant. This sequence of events may represent a progression from aberrant protein aggregation and initial autophagy impairment to autophagy decompensation.

But the interplay between TDP-43 and ANXA11 within the cytoplasm is complex and warrants closer examination. Our observations reveal co-localization of TDP-43, ANXA11, and p62, suggesting a potential cooperative or synergistic role. However, the precise mechanistic relationship remains unclear. We propose that mutant ANXA11 (mANXA11) actively attracts TDP-43 to facilitate the degradation of aggregates. This hypothesis is supported by two lines of evidence. First, TDP-43 inclusions are extensively observed in both familial and sporadic cases of disease and consistently co-localize with p62, a key mediator in protein degradation processes essential for maintaining cellular homeostasis. In fact, p62 mitigates TDP-43 aggregation in an autophagy- and proteasome-dependent manner [51]. This supports the notion that TDP-43 may engage with mANXA11 as part of a downstream degradation mechanism. Second, while ANXA11 has been shown to bind RNA and lysosomes via its phase-separating and membrane-binding domains, these tethering functions are impaired in mANXA11 [52]. Consequently, the ability of mANXA11 to mediate active lysosomal degradation of aggregates is likely compromised. These findings collectively underscore

the potential role of TDP-43 in recruiting mANXA11 for aggregate management, albeit through an impaired degradation pathway.

MTOR activation is a master negative regulator of autophagy. Under neurodegenerative conditions, inhibition of mTORC1, will stimulate autophagy and the removal of misfolded proteins [53]. In our *ANXA11*-mutant mice model, activation of MTOR-AKT-P70S6K pathway coincided with autophagy impairment. The nature of this response in the disease process remains unclear, as mTOR inhibition has yielded contradictory results. On one hand, mTOR inhibition reduces TDP-43 aggregation and toxicity in multiple ALS models [49]; on the other, rapamycin has been shown to facilitate motor neuron degeneration and accelerate disease progression in *SOD1*-G93A ALS mice [54]. Overall, the role of autophagy impairment and mTOR activation in *ANXA11* mutant mice, whether this response is beneficial or maladaptive, remains incompletely defined.

Lastly, the interplay between inflammation and autophagy impairment in ALS is intricate. Motor neuron degeneration in ALS involves multiple cell-autonomous mechanisms, such as protein misfolding, oxidative stress, mitochondrial dysfunction, and disrupted RNA metabolism [55], all of which trigger non-cell-autonomous inflammatory responses. Inflammatory mediators, in turn, exacerbate neuronal damage, creating a self-perpetuating cycle where inflammation becomes a secondary consequence of neurodegeneration. Moreover, these mediators directly interfere with autophagy by suppressing autophagy-related genes, disrupting autophagosome-lysosome fusion, and inducing metabolic dysregulation, which further impairs autophagy. This suggests a bidirectional relationship in which inflammation and autophagy dysfunction mutually amplify disease progression. We observed that neuroinflammation and autophagy impairment occur at the same disease stages (Fig. 9), highlighting the challenge of translating strategies targeting either pathway into clinical therapies for ALS.

Conclusions

We have established an *ANXA11*-P36R knock-in ALS mice that recapitulates the phenotypes patients with this mutation, including late-onset disease and extended survival. The *ANXA11*-P36R mutation, located in the LCD, induces TDP-43 proteinopathy, neuroinflammation, stress granule misprocessing, and autophagic dysfunction.

Abbreviations

ALS	Amyotrophic lateral sclerosis
LCD	Low-complexity domain
FTD	Frontotemporal dementia
CNS	Central nervous system
NOR	Novel object recognition
OFT	Open field tests
EPM	Elevated plus maze
ROI	Region of interest
wt	Wild-type
CMAPs	Compound muscle action potentials
HE	Hematoxylin and eosin
NADH-TR	NADH tetrazolium reductase
het	Heterozygous
hom	Homozygous
mo	Months
MNs	Motor neurons

Supplementary Information

The online version contains supplementary material available at https://doi.org/10.1186/s40478-024-01919-4.

Additional file 1.

Additional file 2.

Additional file 3.

Acknowledgements

We thank Dr. Ling Zhang and Yuanwu Ma for advices in animal behavior tests.

Author contributions

Liu Q supervised the study, analyzed most of the data and presented with figures, wrote most part of the article and revised the manuscript; He B and Sun Y performed part of immunostaining, took the images (Figs. 2–6), analyzed neuropathological data, and wrote part of the article (Table 1); Zhang K and Zhao X help established the knock-in mice; Chen H, Wang L, Wang G and Zhang XZ managed the mice, performed and analyzed behavior tests, and did the molecular biological tests (data of Fig. 1, Figs. 7 and 8); Shen D followed up the patient and gave the clinical data; Liying Cui, and Xue Zhang supervised the study. All authors reviewed the manuscript.

Funding

This work was supported by National Key Research and Development Program [2022YFC2703904, 2022YFC2703900], Strategic Priority Research Program (Pilot study) "Biological basis of aging and therapeutic strategies" of the Chinese Academy of Sciences [XDB39040000], the Chinese Academy of Medical Sciences (CAMS) Innovation Fund for Medical Sciences [2021-I2M-1-034, 2021-I2M-1-018], National High Level Hospital Clinical Research Funding [2022-PUMCH-B-017], and National Natural Science Foundation of China[81971293, 82201562].

Availability of data and materials

The authors confirm that the data supporting the findings of this study are available within the article and its Supplementary Material.

Declarations

Ethics approval and consent to participate

The study complies with the Institutional Animal Care and Use Committee (IACUC) guidelines at Peking Union Medical College Hospital, adhering to the Guide for the Care and Use of Laboratory Animals (Eighth Edition, NHR).

Consent for publication

Not applicable.

Competing interests

The authors declare no competing interests.

Author details

[1]Department of Neurology, Peking Union Medical College Hospital, Peking Union Medical College (PUMC) and Chinese Academy of Medical Science (CAMS), Beijing, China. [2]Department of Neurology, Beijing Tiantan Hospital, Capital Medical University, Beijing, China. [3]China National Clinical Research Center for Neurological Diseases, Beijing, China. [4]State Key Laboratory

of Medical Molecular Biology, Mckusick-Zhang Center for Genetic Medicine, Institute of Basic Medical Sciences, PUMC and CAMS, Beijing, China. [5]State Key Laboratory of Complex, Severe, and Rare Diseases, PUMCH, Beijing, China.

Received: 27 August 2024 Accepted: 20 December 2024
Published online: 04 January 2025

References

1. Nahm M, Lim SM, Kim YE, Park J, Noh MY, Lee S et al (2020) ANXA11 mutations in ALS cause dysregulation of calcium homeostasis and stress granule dynamics. Sci Transl Med. https://doi.org/10.1126/scitranslmed.aax3993
2. Leoni TB, Gonzalez-Salazar C, Rezende TJR, Hernandez ALC, Mattos AHB, Coimbra Neto AR et al (2021) A novel multisystem proteinopathy caused by a missense ANXA11 variant. Ann Neurol 90(2):239–252. https://doi.org/10.1002/ana.26136
3. Sung W, Nahm M, Lim SM, Noh MY, Lee S, Hwang SM et al (2022) Clinical and genetic characteristics of amyotrophic lateral sclerosis patients with ANXA11 variants. Brain Commun. https://doi.org/10.1093/braincomms/fcac299
4. Wang Y, Duan X, Zhou X, Wang R, Zhang X, Cao Z et al (2022) ANXA11 mutations are associated with amyotrophic lateral sclerosis-frontotemporal dementia. Front Neurol 13:886887. https://doi.org/10.3389/fneur.2022.886887
5. Zhang K, Liu Q, Liu K, Shen D, Tai H, Shu S et al (2018) ANXA11 mutations prevail in Chinese ALS patients with and without cognitive dementia. Neurol Genet. https://doi.org/10.1212/NXG.0000000000000237
6. Zhang X, Gao J, Chi C, Zhao Z, Chan P, Ma J (2023) An atypical ALS with PSP-like symptoms caused by ANXA11 p.D40G mutation: a case report and literature review. Front Neurol 14:1086264
7. Jiang Q, Lin J, Wei Q, Li C, Hou Y, Cao B et al (2022) Genetic analysis of and clinical characteristics associated with ANXA11 variants in a Chinese cohort with amyotrophic lateral sclerosis. Neurobiol Dis 175:105907. https://doi.org/10.1016/j.nbd.2022.105907
8. Platt RJ, Chen S, Zhou Y, Yim MJ, Swiech L, Kempton HR et al (2014) CRISPR-Cas9 knockin mice for genome editing and cancer modeling. Cell 159(2):440–455. https://doi.org/10.1016/j.cell.2014.09.014
9. Shalem O, Sanjana NE, Zhang F (2015) High-throughput functional genomics using CRISPR-Cas9. Nat Rev Genet 16(5):299–311. https://doi.org/10.1038/nrg3899
10. Chew J, Gendron TF, Prudencio M, Sasaguri H, Zhang YJ, Castanedes-Casey M et al (2015) C9ORF72 repeat expansions in mice cause TDP-43 pathology, neuronal loss, and behavioral deficits. Science 348(6239):1151–1154. https://doi.org/10.1126/science.aaa9344
11. Pentkowski NS, Rogge-Obando KK, Donaldson TN, Bouquin SJ, Clark BJ (2021) Anxiety and Alzheimer's disease: Behavioral analysis and neural basis in rodent models of Alzheimer's-related neuropathology. Neurosci Biobehav Rev 127:647–658. https://doi.org/10.1016/j.neubiorev.2021.05.005
12. Takagi T, Nishizaki Y, Matsui F, Wakamatsu N, Higashi Y (2015) De novo inbred heterozygous Zeb2/Sip1 mutant mice uniquely generated by germ-line conditional knockout exhibit craniofacial, callosal and behavioral defects associated with Mowat-Wilson syndrome. Hum Mol Genet 24(22):6390–6402. https://doi.org/10.1093/hmg/ddv350
13. Hughes RN (2004) The value of spontaneous alternation behavior (SAB) as a test of retention in pharmacological investigations of memory. Neurosci Biobehav Rev 28(5):497–505. https://doi.org/10.1016/j.neubiorev.2004.06.006
14. Dubowitz V, Sewry CA. Muscle biopsy: A practical approach. 3rd ed. Elsevier, Philadelphia.
15. Ma HR, Wang SB, Wang F, Gong M, Zhang QY, Song SN et al (2020) Frontotemporal dementia with ANXA11 gene mutation: a case report and literature review. Chin J Neurol 53(10):772–776. https://doi.org/10.3760/cma.j.cn113694-20200317-00185
16. Johari M, Papadimas G, Papadopoulos C, Xirou S, Kanavaki A, Chrysanthou-Piterou M et al (2022) Adult-onset dominant muscular dystrophy in Greek families caused by Annexin A11. Ann Clin Transl Neurol 9(10):1660–1667. https://doi.org/10.1002/acn3.51665
17. Natera-de Benito D, Olival J, Garcia-Cabau C, Jou C, Roldan M, Codina A et al (2023) Common pathophysiology for ANXA11 disorders caused by aspartate 40 variants. Ann Clin Transl Neurol 10(3):408–425. https://doi.org/10.1002/acn3.51731
18. Robinson JL, Suh E, Xu Y, Hurtig HI, Elman L, McMillan CT et al (2024) Annexin A11 aggregation in FTLD-TDP type C and related neurodegenerative disease proteinopathies. Acta Neuropathol 147(1):104. https://doi.org/10.1007/s00401-024-02753-7
19. Liu WJ, Ye L, Huang WF, Guo LJ, Xu ZG, Wu HL et al (2016) p62 links the autophagy pathway and the ubiquitin-proteasome system upon ubiquitinated protein degradation. Cell Mol Biol Lett 21:29. https://doi.org/10.1186/s11658-016-0031-z
20. Komatsu M, Kurokawa H, Waguri S, Taguchi K, Kobayashi A, Ichimura Y et al (2010) The selective autophagy substrate p62 activates the stress responsive transcription factor Nrf2 through inactivation of Keap1. Nat Cell Biol 12(3):213–223. https://doi.org/10.1038/ncb2021
21. Cook CN, Wu Y, Odeh HM, Gendron TF, Jansen-West K, Del Rosso G et al (2020) C9orf72 poly(GR) aggregation induces TDP-43 proteinopathy. Sci Transl Med. https://doi.org/10.1126/scitranslmed.abb3774
22. Mackenzie IR, Bigio EH, Ince PG, Geser F, Revesz T, Robinson JL et al (2011) A harmonized classification system for FTLD-TDP pathology. Acta Neuropathol 122(1):111–113. https://doi.org/10.1007/s00401-011-0845-8
23. Alami NH, Smith RB, Carrasco MA, Williams LA, Winborn CS, Han SS-W et al (2014) Axonal transport of TDP-43 mRNA granules is impaired by ALS-causing mutations. Neuron 81(3):536–543
24. Liao YC, Fernandopulle MS, Wang G, Choi H, Hao L, Drerup CM et al (2019) RNA granules hitchhike on lysosomes for long-distance transport, using Annexin A11 as a molecular tether. Cell 179(1):147-164.e20. https://doi.org/10.1016/j.cell.2019.08.050
25. Sainouchi M, Hatano Y, Tada M, Ishihara T, Ando S, Kato T et al (2021) A novel splicing variant of ANXA11 in a patient with amyotrophic lateral sclerosis: histologic and biochemical features. Acta Neuropathol Commun 9(1):106. https://doi.org/10.1186/s40478-021-01202-w
26. Teyssou E, Muratet F, Amador MD, Ferrien M, Lautrette G, Machat S et al (2021) Genetic screening of ANXA11 revealed novel mutations linked to amyotrophic lateral sclerosis. Neurobiol Aging. https://doi.org/10.1016/j.neurobiolaging.2020.10.015
27. Guttenplan KA, Weigel MK, Adler DI, Couthouis J, Liddelow SA, Gitler AD et al (2020) Knockout of reactive astrocyte activating factors slows disease progression in an ALS mouse model. Nat Commun 11(1):3753. https://doi.org/10.1038/s41467-020-17514-9
28. Woodburn SC, Bollinger JL, Wohleb ES (2021) The semantics of microglia activation: neuroinflammation, homeostasis, and stress. J Neuroinflammation 18(1):258. https://doi.org/10.1186/s12974-021-02309-6
29. Rabanal-Ruiz Y, Otten EG, Korolchuk VI (2017) mTORC1 as the main gateway to autophagy. Essays Biochem 61(6):565–584. https://doi.org/10.1042/EBC20170027
30. Laplante M, Sabatini DM (2013) Regulation of mTORC1 and its impact on gene expression at a glance. J Cell Sci 126(Pt 8):1713–1719. https://doi.org/10.1242/jcs.125773
31. Gurney ME, Pu H, Chiu AY, Dal Canto MC, Polchow CY, Alexander DD et al (1994) Motor neuron degeneration in mice that express a human Cu,Zn superoxide dismutase Mutation. Science 264(5166):1772–1775. https://doi.org/10.1126/science.8209258
32. Wang Y, Duan X, Zhou X, Wang R, Zhang X, Cao Z et al (2022) ANXA11 mutations are associated with amyotrophic lateral sclerosis-frontotemporal dementia. Front Neurol 13:886887
33. Mori F, Tada M, Kon T, Miki Y, Tanji K, Kurotaki H et al (2019) Phosphorylated TDP-43 aggregates in skeletal and cardiac muscle are a marker of myogenic degeneration in amyotrophic lateral sclerosis and various conditions. Acta Neuropathol Commun 7(1):165
34. Aishwarya R, Abdullah CS, Remex NS, Nitu S, Hartman B, King J et al (2023) Pathological Sequelae associated with skeletal muscle atrophy and histopathology in G93A*SOD1 mice. Muscles 2(1):51–74
35. Weishaupt JH, Hyman T, Dikic I (2016) Common molecular pathways in amyotrophic lateral sclerosis and frontotemporal dementia. Trends Mol Med 22(9):769–783. https://doi.org/10.1016/j.molmed.2016.07.005
36. Wolozin B, Ivanov P (2019) Stress granules and neurodegeneration. Nat Rev Neurosci 20(11):649–666. https://doi.org/10.1038/s41583-019-0222-5

37. Zbinden A, Perez-Berlanga M, De Rossi P, Polymenidou M (2020) Phase separation and neurodegenerative diseases: a disturbance in the force. Dev Cell 55(1):45–68. https://doi.org/10.1016/j.devcel.2020.09.014
38. Kroschwald S, Alberti S (2017) Gel or die: phase separation as a survival strategy. Cell 168(6):947–948. https://doi.org/10.1016/j.cell.2017.02.029
39. Yang P, Mathieu C, Kolaitis RM, Zhang P, Messing J, Yurtsever U et al (2020) G3BP1 is a tunable switch that triggers phase separation to assemble stress granules. Cell 181(2):325-345.e28. https://doi.org/10.1016/j.cell.2020.03.046
40. Zhang K, Daigle JG, Cunningham KM, Coyne AN, Ruan K, Grima JC et al (2018) Stress granule assembly disrupts nucleocytoplasmic transport. Cell 173(4):958-971.e17. https://doi.org/10.1016/j.cell.2018.03.025
41. Li YR, King OD, Shorter J, Gitler AD (2013) Stress granules as crucibles of ALS pathogenesis. J Cell Biol 201(3):361–372. https://doi.org/10.1083/jcb.201302044
42. Zhang X, Wang F, Hu Y, Chen R, Meng D, Guo L et al (2020) In vivo stress granule misprocessing evidenced in a FUS knock-in ALS mouse model. Brain 143(5):1350–1367. https://doi.org/10.1093/brain/awaa076
43. Babazadeh A, Rayner SL, Lee A, Chung RS (2023) TDP-43 as a therapeutic target in neurodegenerative diseases: Focusing on motor neuron disease and frontotemporal dementia. Ageing Res Rev 92:102085. https://doi.org/10.1016/j.arr.2023.102085
44. Neumann M, Sampathu DM, Kwong LK, Truax AC, Micsenyi MC, Chou TT et al (2006) Ubiquitinated TDP-43 in frontotemporal lobar degeneration and amyotrophic lateral sclerosis. Science 314(5796):130–133. https://doi.org/10.1126/science.1134108
45. Liao YZ, Ma J, Dou JZ (2022) The role of TDP-43 in neurodegenerative disease. Mol Neurobiol 59(7):4223–4241. https://doi.org/10.1007/s12035-022-02847-x
46. Ke YD, van Hummel A, Stevens CH, Gladbach A, Ippati S, Bi M et al (2015) Short-term suppression of A315T mutant human TDP-43 expression improves functional deficits in a novel inducible transgenic mouse model of FTLD-TDP and ALS. Acta Neuropathol 130(5):661–678. https://doi.org/10.1007/s00401-015-1486-0
47. Walker AK, Spiller KJ, Ge G, Zheng A, Xu Y, Zhou M et al (2015) Functional recovery in new mouse models of ALS/FTLD after clearance of pathological cytoplasmic TDP-43. Acta Neuropathol 130(5):643–660. https://doi.org/10.1007/s00401-015-1460-x
48. Chua JP, De Calbiac H, Kabashi E, Barmada SJ (2022) Autophagy and ALS: mechanistic insights and therapeutic implications. Autophagy 18(2):254–282. https://doi.org/10.1080/15548627.2021.1926656
49. Sasaki S (2011) Autophagy in spinal cord motor neurons in sporadic amyotrophic lateral sclerosis. J Neuropathol Exp Neurol 70(5):349–359. https://doi.org/10.1097/NEN.0b013e3182160690
50. Klionsky DJ, Abdelmohsen K, Abe A, Abedin MJ, Abeliovich H, Acevedo Arozena A, et al (2016) Guidelines for the use and interpretation of assays for monitoring autophagy (3rd edition). Autophagy https://doi.org/10.1080/15548627.2015.1100356.
51. Brady OA, Meng P, Zheng Y, Mao Y, Hu F (2011) Regulation of TDP-43 aggregation by phosphorylation and p62/SQSTM1. J Neurochem. 116(2):248–59
52. Arseni D, Nonaka T, Jacobsen MH, Murzin AG, Cracco L, Peak-Chew SY et al (2024) Heteromeric amyloid filaments of ANXA11 and TDP-43 in FTLD-TDP type C. Nature 634(8034):662–668
53. Querfurth HW, Lee HK (2021) Mammalian/mechanistic target of rapamycin (mTOR) complexes in neurodegeneration. Mol Neurodegener 16(1):44. https://doi.org/10.1186/s13024-021-00428-5
54. Zhang X, Li L, Chen S, Yang D, Wang Y, Zhang X et al (2011) Rapamycin treatment augments motor neuron degeneration in SOD1(G93A) mouse model of amyotrophic lateral sclerosis. Autophagy 7(4):412–425. https://doi.org/10.4161/auto.7.4.14541
55. Appel SH, Beers DR, Zhao W (2021) Amyotrophic lateral sclerosis is a systemic disease: peripheral contributions to inflammation-mediated neurodegeneration. Curr Opin Neurol 34(5):765–772

Publisher's Note